DEUTSCHES ELEKTRONEN – SYNCHROTRON

DESY 92-073
May 1992

Photon Induced Reactions at HERA

A. Levy

Deutsches Elektronen-Synchrotron DESY, Hamburg

and

School of Physics, Tel-Aviv University, Israel

ISSN 0418-9833

NOTKESTRASSE 85 · D-2000 HAMBURG 52

DESY 92-073
May 1992

ISSN 0418-9833

Photon induced reactions at HERA [1]

Aharon Levy

Deutsches Elektronen-Synchrotron, DESY
and
School of Physics, Tel-Aviv University

ABSTRACT

Some phenomenological and experimental issues concerning photoproduction at HERA are discussed. This includes the total photoproduction cross section, light and heavy quark photoproduction, determination of parton densities in the proton and in the photon and the photon-photon possibilities at HERA.

1 Introduction

HERA is expected to start data taking soon and there is a growing excitement to see the first physics results. The potential of HERA is immense [1]. The low x physics will enable the study of saturation of partons in the proton, with the possibility to look for hot spots [2]. The high Q^2 events will serve as a check of the validity of QCD in kinematic regions far beyond the presently accessible ones and will allow the study of substructure of the elementary constituents of matter [3]. HERA is the ideal machine for the search of leptoquarks and other exotic phenomena like the search for flavour changing neutral currents [4]. The accelerator has achieved a polarization of the electron beam of $\sim 20\%$ already at a very early stage and with the hope that higher stable polarization is achieved one can have very interesting additional information from polarized electrons colliding with protons [5]. The low Q^2 physics will extend the study of photoproduction to very high energies and allow a deeper insight in the behaviour of the photon [6]. In addition to all these, HERA will provide the input needed for calculating the expectations from the future colliders like LHC and SSC.

In this talk I will concentrate on the very low Q^2 region and discuss what we can learn from and about the photon at HERA. Before doing that let me recasp how we view the photon, based on what we have learned so far from γp [7] and $\gamma\gamma$ [8] experiments. The photon is a gauge particle mediating electromagnetic interactions. As such it couples to the elementary charged constituents of matter, like leptons and quarks, in a well defined way. However, the photon may also exhibit properties similar to normal hadrons. When one studies the soft photoproduction reactions, they are well described by assuming a model in which the photon is a superposition of vector mesons [9] (figure 1a). When one 'looks' at the photon with a highly virtual photon in $\gamma\gamma$ reactions, the notion of the photon structure function is introduced in analogy to the well known nucleon case. This photon structure function has indeed been measured experimentally and can be interpreted in terms of parton distributions in the photon [10]. When the photon participates in a hard interaction it will either couple directly to the charged constituents of matter as shown in figure 1b (**direct photon**), or first fragment into quarks and gluons which in turn participate in the hard process, as shown in figures 1c and 1d. Whenever the photon turns into partons before interacting, be it through point-like couplings or with hadron-like couplings, it is called a **resolved photon**. Direct photon reactions are usually used to study the structure of the proton while the resolved photon ones contain information about partons in the photon [10].

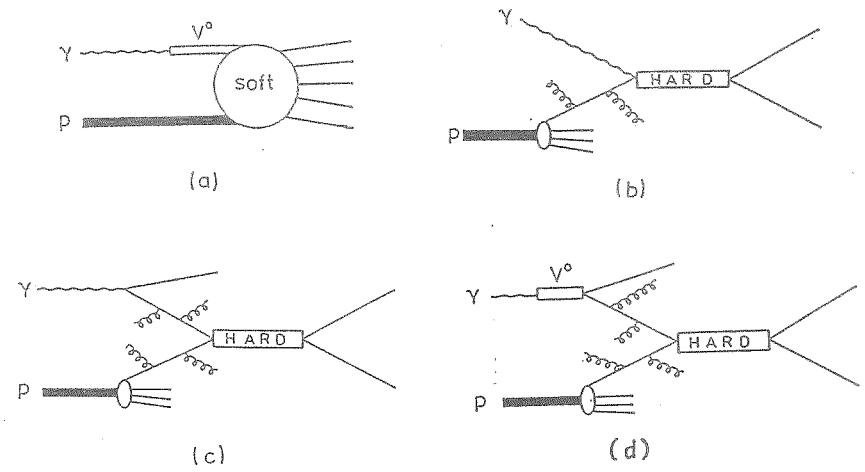

Figure 1: a) Diagram for a soft $\gamma p \rightarrow$ hadrons reaction. b)–d): Diagrams for a γp hard process. b) A direct photon contribution to 2–jet production. c) The point–like contribution to the resolved photon contribution to 2–jet production. d) The hadron–like contribution to the resolved photon contribution to 2–jet production.

In this review I discuss four sub–topics, all in the photoproduction range of HERA. The next section contains the predictions for the total photoproduction cross section at HERA and the possibility to measure it experimentally. Section 3 is devoted to light and heavy quark photoproduction, where the dependence of the cross section on the different parametrizations and on the assumed scale is discussed. Attempts to separate resolved photon from direct photon events as well as to distinguish between quark and gluon jets are also described. The subsequent section is about the determination of the gluon density in the proton, via photoproduction of J/Ψ and D^*'s, and about that in the photon via the Deep Inelastic Compton (DIC) process. In the final section, the possibility of detecting $\gamma\gamma$ reactions at HERA is explored.

[1] Talk presented at the 9th International Workshop on Photon–Photon Collisions, La Jolla, 23–26 March, 1992.

2 The total photoproduction cross section

2.1 Theoretical predictions

There exist various predictions for the value of the total photoproduction cross section at high energies. These can be classified as either based on a phenomenological Regge–type approach [11,12], or as a perturbative QCD one [13,14,15,16,17].

2.1.1 Regge–type approach

The prediction of reference 2 is the result of a phenomenological and numerical description of the cross section for photon–proton interactions in the whole range of photon virtualities, from $Q^2 = 0$ to the highest Q^2 values available experimentally. The search for a smooth transition from the deep inelastic scattering (DIS) region to that of $Q^2 = 0$ has two reasons. From a purely practical point of view a parametrization of the γp cross section in a large range of Q^2, starting from the real photon cross section, is very useful for estimating acceptance corrections and radiative corrections for all experiments on leptoproduction. From the theoretical point of view it is of interest to see whether experimentally the interactions of virtual photons of small virtuality display similar properties as hadron–hadron interactions. The possibility of a unified description of the small (soft processes) and high (hard processes) virtuality "photoproduction" cross sections may shed some light on the transition between the soft strong interactions and the hard interactions described in terms of perturbative QCD.

Use is made of the fact that the total γp photoproduction cross section can be well described by the exchange of a Pomeron and a Reggeon trajectory [18]:

$$\sigma_{tot}(\gamma p) = \sigma^o_{\mathcal{P}} s^{\alpha_{\mathcal{P}}-1} + \sigma^o_{\mathcal{R}} s^{\alpha_{\mathcal{R}}-1} \tag{1}$$

where s is the center of mass energy squared, and $\alpha_{\mathcal{P}}$ and $\alpha_{\mathcal{R}}$ denote the Pomeron and Reggeon intercepts, respectively. It has been pointed out [19] that the cross section for virtual photon–proton scattering can be described in a similar Regge language, provided threshold effects arising from the presence of a virtual particle in the scattering process are taken into account.

In the deep inelastic region, the Regge language can be translated into the parton language, in the sense that the sea content of the proton determines the Pomeron contribution to the absorption cross section and the valence content of the proton determines that of the Reggeon. Thus, the total absorption cross section for virtual photon, γ^*, scattering off the proton can be written as a sum of two contributions:

$$\sigma_{tot}(\gamma^* p) = \sigma^*_{\mathcal{P}}(Q^2) + \sigma^*_{\mathcal{R}}(Q^2) \tag{2}$$

Notice that the low Bjorken x region of the parton language corresponds to large energies s and small virtualities Q^2, a region relevant for the application of the Regge language. At the same time the low x measurements can be used as a constraint for the high energy photoproduction cross section.

The following parametrization has been used:

$$\sigma_T(\gamma^{(*)} p) = \frac{4\pi^2\alpha}{Q^2 + m_0^2}\frac{1}{1-x}\left(1 + \frac{4m_p^2 Q^2}{(Q^2 + W^2 - m_p^2)^2}\right)(F_2^{\mathcal{P}} + F_2^{\mathcal{R}}) \tag{3}$$

where

$$F_2^{\mathcal{P}} = C_{\mathcal{P}}(t) x_{\mathcal{P}}^{a_{\mathcal{P}}(t)}(1-x)^{b_{\mathcal{P}}(t)} \tag{4}$$

$$F_2^{\mathcal{R}} = C_{\mathcal{R}}(t) x_{\mathcal{R}}^{a_{\mathcal{R}}(t)}(1-x)^{b_{\mathcal{R}}(t)} \tag{5}$$

and t is defined so as to make it applicable also at $Q^2 = 0$.

$$t = \ln\left(\frac{\ln\left(\frac{Q^2+Q_c^2}{\Lambda^2}\right)}{\ln\left(\frac{Q_0^2}{\Lambda^2}\right)}\right) \tag{6}$$

The two mass scales $m_{\mathcal{P}}$ and $m_{\mathcal{R}}$ are related to $x_{\mathcal{P}}$ and $x_{\mathcal{R}}$ via the equations:

$$\frac{1}{x_{\mathcal{P}}} = 1 + \frac{W^2 - m_p^2}{Q^2 + m_{\mathcal{P}}^2} \tag{7}$$

and

$$\frac{1}{x_{\mathcal{R}}} = 1 + \frac{W^2 - m_p^2}{Q^2 + m_{\mathcal{R}}^2} \tag{8}$$

All available total γp cross section data above $W = 1.75$ GeV have been used, thus avoiding the resonance region. The data used for $\gamma^* p$ interactions were those of the NA28 and BCDMS experiments on μp scattering and of the SLAC experiment on ep scattering.

The results of this parametrization (ALLM [12]) are shown in figure 2 for the total cross section of real photons, and in figure 3 for the DIS region. The parametrization

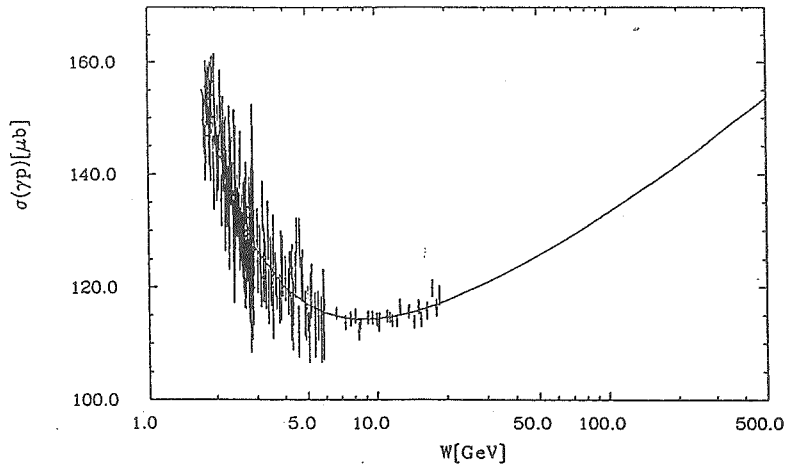

Figure 2: Comparison between the total γp cross section as measured for the real photon and the fit results of ALLM.

extrapolates smoothly into the resonance region, $W < 1.75$ GeV, described by the parametrization of Brasse et al. [20]. It also agrees at higher values of Q^2, where no data are available, with the predictions of some parametrizations obtained as a result of the evolution of parton densities through the standard QCD evolution equations (see figure 3).

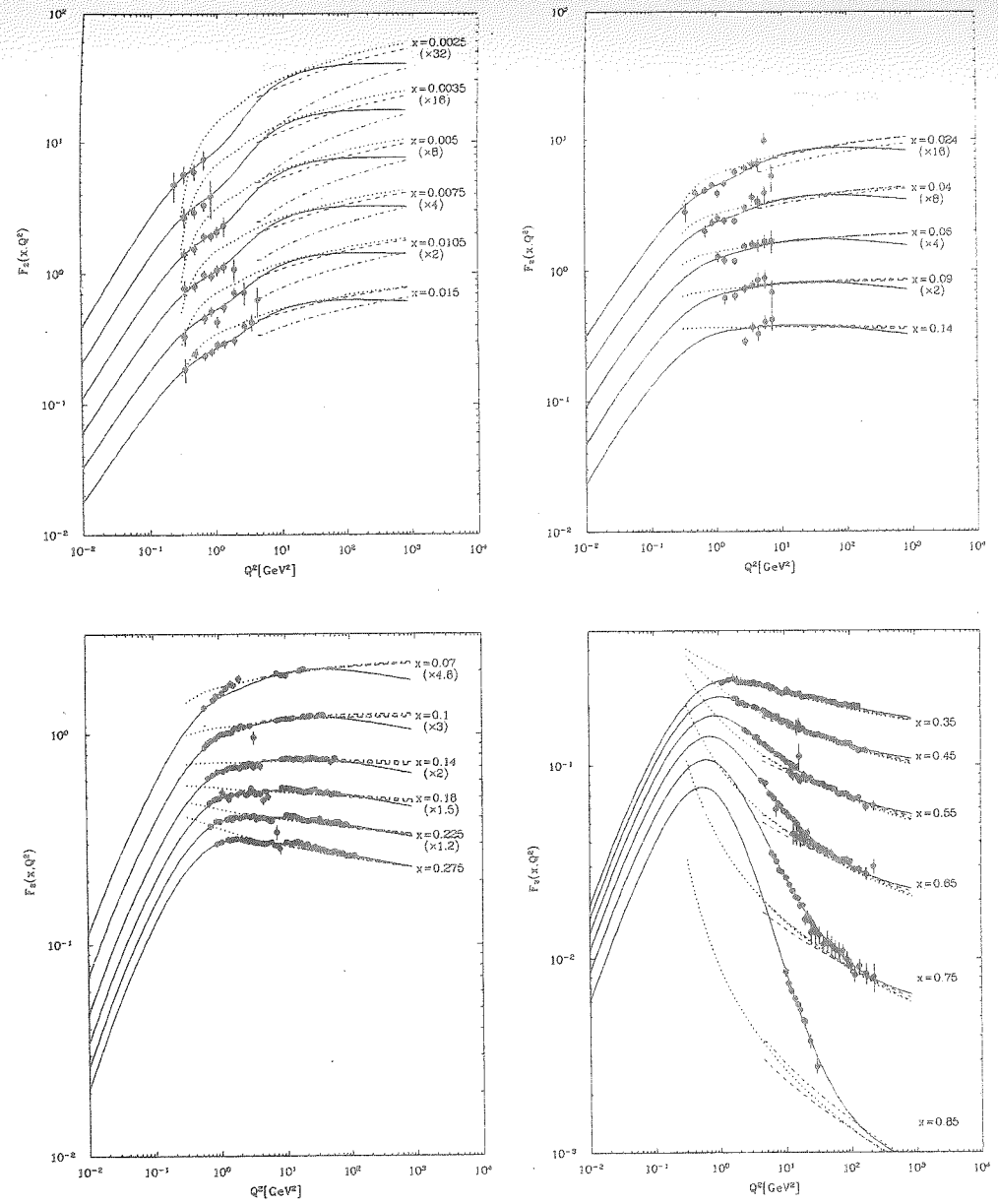

Figure 3: Comparison of the prediction of the ALLM parametrization (full line) with the predictions of the dynamical GRV (dotted line), the KMRS (dashed–dotted line) and the MT (dashed line) parametrizations for F_2 as a function of Q^2, for fixed values of x (see text for more details). The data are superimposed to underline the kinematical region probed by measurements.

This Regge type of phenomenological approach predicts a value of $\sim$ 145 μb for the total γp cross section at $W \sim 200$ GeV. It is to be compared to $\sim$175 μb, obtained in a similar approach based on older data in reference [11].

2.1.2 Perturbative QCD approach

The rise of the total photoproduction cross section is expected to happen as a result of the onset of QCD minijets. The total inelastic γp cross section is assumed to have an energy independent part, coming from the soft non–perturbative interactions, and a QCD part which rises with energy due to the rapid increase of gluons in the proton and in the photon. The latter part includes contributions both from the direct and from the resolved photon:

$$\sigma_{inel}(s) = \sigma_{inel}^{soft} + \sigma_{inel}^{QCD}(s) \tag{9}$$

where,

$$\sigma_{inel}^{QCD}(s) = \sigma_{inel}^{dir}(s) + \sigma_{inel}^{res}(s) \tag{10}$$

However, in order not to violate unitarity, one transforms to the impact parameter representation and assumes that the eikonal is additive and not the cross section:

$$\sigma_{inel}(s) = \int d^2b(1 - e^{-2\chi(b,s)}) \tag{11}$$

where

$$\chi(b,s) = \chi^{soft}(b) + \chi^{QCD}(b,s) \tag{12}$$

This needs further modifications to take into account correctly the hadronic nature of the photon details of which can be found in [16].

Predictions based on this approach depend on the parton parametrizations and on p_T^{min}, the minimal transverse momentum down to which the perturbative calculation is assumed to be valid. Figure 4 shows the predictions based on the minijet approach as calculated in [13], for different parameters. The predictions for the total photoproduction cross section get as high as $760\mu b$ in the HERA energy range. The same authors also calculate the cross section for the 'elastic' photoproduction reaction $\gamma p \rightarrow \rho^0 p$ and predict cross sections in the range of $20 - 220\mu b$ [13].

2.2 Experimental measurement of $\sigma_T(\gamma p)$ at HERA

The best way to measure the total photoproduction cross section at HERA would be in principle to use the luminosity monitor system. The electron tagger can provide information on the exchanged photon energy and on its virtuality Q^2. Though the electron tagger can detect the energy of the electrons scattered under $\theta < 6$mrad and in the range $5 < E' < 25$ GeV, its acceptance is optimal for $15 < E' < 20$ GeV. This is also the range for which the Q^2 resolution is the best and is $\sim$ 10-20% [21,22].

There are two sources of background which make this method of direct measurement impractical: the electron–proton bremsstrahlung and the beam–gas bremsstrahlung, both of which are expected to have much higher cross section in the photon energy range of interest. In principle one could eliminate the first source by detecting the bremsstrahlung photon in the forward photon detector of the luminosity monitor. Even though the acceptance of the photon detector is 97%, this background is reduced only

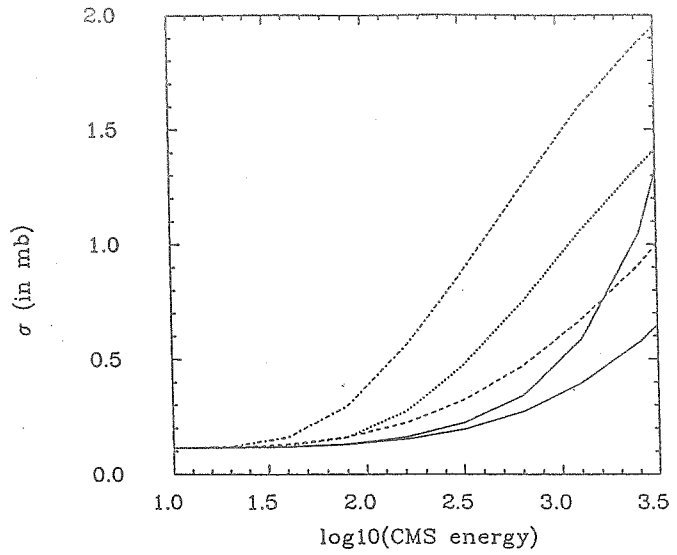

Figure 4: Center-of-mass energy dependence of the total photon–proton cross section in the minijet approach using KMRS (proton) and DG or LAC (photon) parton distributions and taking $p^2_{Tmin} = 2$ or $4\,\mathrm{GeV}^2$. Dotted (dot-dashed) line, eikonal using LAC1 and $p^2_{Tmin} = 4\,\mathrm{GeV}^2$ ($2\,\mathrm{GeV}^2$); lower solid (dashed) line, eikonal using DG and $p^2_{Tmin} = 4\,\mathrm{GeV}^2$ ($2\,\mathrm{GeV}^2$); upper solid line, additive model using DG and $p^2_{Tmin} = 4\,\mathrm{GeV}^2$.

by a factor of ~ 50. The beam–gas background can be reduced by the photon detector only when the interaction of the beam with the gas happens in the straight section.

In order to be somewhat more quantitative, we present the calculation given in reference [23]. An incoming electron of energy $E = 30$ GeVand a scattered electron with energy $E' = 15 - 20$ GeV will produce photons with $k = E - E' = 10 - 15$ GeV. The observable cross section will be

$$\int_{k_1}^{k_2} d\sigma_T(ep) = \int_{k_1}^{k_2} \sigma_T(\gamma p) dF \tag{13}$$

By using the Weizsäcker–Williams formula [24,25] for the flux factor dF, and assuming $\sigma_T(\gamma p) = 145\mu$b [12] in this photon energy range, one obtains

$$\int_{10}^{15} d\sigma_T(ep) = 0.65\mu\mathrm{b} \tag{14}$$

By using the complete energy range of the scattered electron, one can get a cross section of 2.2μb.

The cross section for electron–proton bremsstrahlung photons is

$$\int_{10}^{15} d\sigma(ep \to ep\gamma) = 17\mathrm{mb} \tag{15}$$

The contribution of the beam–gas events depends on the rest gas pressure, on its composition, and when assuming a mean atomic Z of 4 and a pressure of 5×10^{-10}mbar, the

rate of this background is equal to that of the electron–proton bremsstrahlung [22]. One would have hoped that since the signal and the two background processes have different Q^2 behaviour, a Q^2 cut could improve the situation. However, as shown in [22], such a cut does not help. One is therefore led to the conclusion that only a coincidence of the luminosity detector together with the main detector could produce a measurable signal of $\sigma_T(\gamma p)$.

Let us continue with the quantitative estimates, assuming for the sake of simplicity that the initial luminosity of the machine would be $10^{30}\mathrm{cm}^{-2}\mathrm{s}^{-1}$ ($\sim 7\%$ of its designed value). The rate of photoproduction events would be 0.6 Hz compared to 17 kHz and 7 kHz from electron–proton and beam–gas bremsstrahlung, respectively. The rate at first level trigger in the main detector will be 46 kHz, assuming a full proton beam [26]. The suggested trigger for measuring $\sigma_T(\gamma p)$ would be a) electron tag and $15 < E' < 20$ GeV, b) a veto from the γ–calorimeter (assumed to be 97% efficient), c) some activity in the main detector. With this procedure the rate of background can be reduced to 3 Hz, compared to the 0.6 Hz of the signal at first level trigger. Further reduction of the background rate can be achieved at the second level trigger, by using a vertex constraint and a simple rapidity cut [23]. This would bring down the background rate to 0.3 Hz. The estimates of reference [21] are somewhat more optimistic and lead to a background rate of 0.1 Hz compared to a signal rate of 1 Hz. Thus one may conclude that it will be possible to measure the total photoproduction cross section at HERA.

The main uncertainty to this measurement will be the systematic error, which in addition to the background will come from the uncertainty in the value of the diffractive part of the cross section, events of which are expected to go mainly unobserved in the beam pipe. Some handle on the measurement of the diffractive part may come from using the Leading Proton Spectrometer (LPS), which is unique to the ZEUS detector, but this is still under study [22]. Another source of difficulty is the large radiative corrections expected. The problem with this correction is that the existing programs to estimate it have not been written with such extreme kinematic limits of so very low Q^2's and scattering electron angles. Nevertheless, in view of the very different predictions for the total photoproduction cross section at HERA energies, even a measurement good to $\sim$ 10–15% of accuracy may already rule out some of the predictions.

3 Light and heavy quark photoproduction

3.1 Cross sections

I would like to discuss in this section the photoproduction of light and heavy quarks. More specifically, it is a study of $2 \to 2$ partonic hard subprocesses leading to final states having two jets. Those produced by a direct photon will have an additional proton remnant jet, while the events coming from a resolved photon will also have the photon remnant jet. Direct photon processes are Photon–Gluon–Fusion (PGF), $\gamma g \to q\bar{q}$, and Compton–QCD (CQCD), $\gamma q \to gq$. The resolved photon processes are $gg \to gg$, $gg \to q\bar{q}$, $qg \to qg$, $q\bar{q} \to gg$, and $q\bar{q} \to q\bar{q}$(see figure 5).

The cross section estimates for these processes depend on quite a few assumptions. The calculation is based on the following expression for the differential cross section:

$$\frac{d\sigma}{dp_T} = 2p_T \int_{\frac{4p_T^2}{s}}^1 dz f_{\gamma/e}(E,z) \int_{\frac{4p_T^2}{s}}^1 dx_a \int_{\frac{4p_T^2}{x_a s}}^1 dx_b f_{q/p}(x_a,\tilde{Q}_2) f_{b/\gamma}(x_b,\tilde{Q}^2) \frac{d\hat{\sigma}}{d\hat{p}_T^2}(\hat{s},\hat{t},\hat{u}) \tag{16}$$

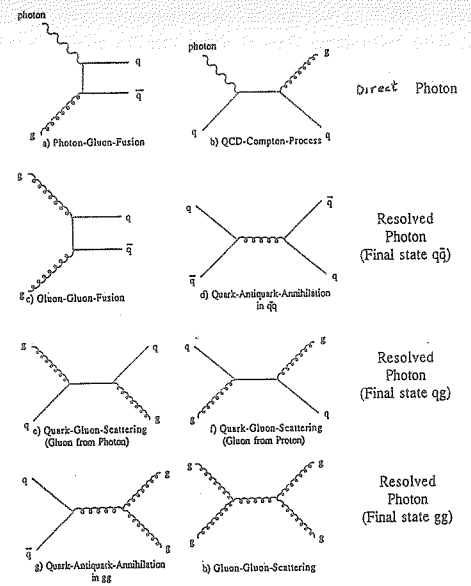

Figure 5: Feynman graphs for hard photoproduction subprocesses due to direct photon interactions (a,b) and due to resolved photon interactions (c–h).

where s is the squared center of mass energy of the ep system. $\hat{s} = zs$ is the center of mass energy squared of the $\gamma^* p$ system, and $\hat{s} = x_a x_b s$ is that of the parton-parton system. The function $f_{\gamma/e}$ is the luminosity factor for the flux of interacting photons originating from the electron beam. The variable $\tilde{Q}^2$ denotes the scale of the hard interaction and should not be mistaken with the absolute value of the squared four-momentum transfer Q^2 from the electron to the nucleon system which determines the virtuality of the photon (which in this case is close to 0). As already mentioned earlier, there is no prescription as to what should be used for $\tilde{Q}^2$, but $\tilde{Q}^2 = p_T^2$ seems to reproduce well the $Sp\bar{p}S$ two-jet data [27]. In the reaction described by the cross section above, the photon can interact either directly or through its own partons and all possible contributions have to be included. In case of the direct photon contribution the following holds:

$$f_{b/\gamma}(x_b, Q^2) = f_{\gamma/\gamma} = \delta(1 - x_b) \qquad (17)$$

In order to check how the different photon parametrizations influence the cross sections of processes which involve the resolved photon, the PYTHIA5.5 generator was used for a comparison between the cross section obtained with the DG [28] and LAC1 [29] parametrization of the parton distributions in the photon, presented in table 1. For completeness also the direct photon reactions are included. Wherever the gluon of the resolved photon participates, the LAC parametrization predicts higher cross sections than the DG one. This is the result of the fact that the gluons of the LAC parametrization have a much larger contribution than the DG one, especially in the low-x region.

Thus the HERA measurements, which extend into this new x domain, will enable the study of the gluon distribution in the photon. The table presents the results for three

Table 1: Comparison between cross sections obtained with the PYTHIA5.5 generator using the DG and the LAC1 parametrizations of the parton distributions in the photon. The MT2 parametrization was used for the proton.

process	σ for different $\hat{p}_T(GeV/c)$ cuts					
	LAC1			DG		
	1	5	10	1	5	10
	$\sigma(\mu b)$	$\sigma(nb)$	$\sigma(pb)$	$\sigma(\mu b)$	$\sigma(nb)$	$\sigma(pb)$
$g+g \to g+g$	385.3	157.1	2.96	26.7	58.1	1.90
$f+g \to f+g$	128.1	159.1	7.04	20.1	92.3	5.52
$g+g \to f+f$	9.16	6.82	0.11	0.57	2.25	0.09
$f+f \to g+g$	0.13	0.68	0.039	0.036	0.47	0.042
$f+f \to f+f$	5.15	56.6	7.06	4.03	51.0	6.64
$\gamma+g \to f+f$	2.94	33.7	3.09	2.98	34.3	3.08
$\gamma+f \to f+g$	0.71	11.9	1.346	0.77	11.5	1.39

different lower cuts of $\hat{p}_T$, and one can see the dramatic drop of the cross section with this cut. Note also that as $\hat{p}_T$ gets higher, the ratio of the direct to resolved photon cross section increases.

Many calculations exist for the cross sections for heavy quark production, like $c\bar{c}$ and $b\bar{b}$ [30]. The hard scattering scale used varies usually from $m_q/2$ to $2m_q$, where m_q is the mass of the heavy quark, which introduces the additional uncertainty of what value to use for the heavy quark mass. Furthermore, the cross section depends on the renormalization scheme giving different results for the DIS and $\overline{MS}$ representations. For the EHLQ parametrization of the proton and DG parametrization for the photon one gets (for $m_c = 1.5GeV$) $\sigma(ep \to c\bar{c}X) = 0.7 \pm 0.2\mu b$ and for $4.5 < m_b < 5.0$ GeV, $\sigma(ep \to b\bar{b}X) = 6.0 \pm 1.1nb$. These values include also higher order corrections [31], the

Table 2: Cross section values for $b\bar{b}$ production for different representations and different hard scattering scales, in order α_s and α_s^2. A value of m_b=4.75 GeVis assumed.

process	$\sigma(ep \to b\bar{b}X)$, nb					
	DIS			$\overline{MS}$		
	$Q = m_b/2$	$Q = m_b$	$Q = 2m_b$	$Q = m_b/2$	$Q = m_b$	$Q = 2m_b$
α_s	0.237	0.190	0.162	0.237	0.190	0.162
$\sigma_{\gamma g} O(\alpha_s)$	4.94	4.60	4.36	4.30	4.16	4.02
$\sigma_{\gamma g} O(\alpha_s^2)$	1.92	1.62	1.72	1.71	1.54	1.68
$\sigma_{\gamma q} O(\alpha_s^2)$	0.92	0.15	-0.21	0.98	0.20	-0.17
$\sigma_{qq} O(\alpha_s^2)$	0.14	0.12	0.11	0.15	0.12	0.11
$\sigma_{gg} O(\alpha_s^2)$	0.85	0.64	0.53	0.73	0.57	0.48
σ_{tot}	8.77	7.13	6.51	7.87	6.59	6.12

effect of which can be seen from table 2. For an expected nominal luminosity of 100 pb^{-1}/year at HERA, one should thus have of the order of 10^8 charm and 10^6 bottom hadrons per year.

3.2 Separation of resolved photon processes

It has been pointed out [32] that photoproduction events produced by resolved photons could be separated from those produced by direct photons due to their different topology. The remnants of the proton will remain mostly in the beam pipe and very little energy is expected in the electron direction for direct photon events. However, in case of the resolved photon events, long range colour forces produce hadrons in the electron direction from the photon remnants (see figure 6). As a result of these colour forces,

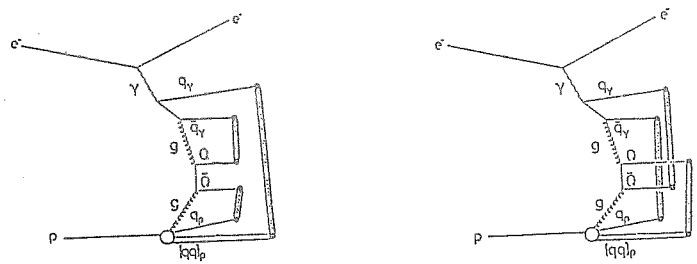

Figure 6: Possible colour recombination for a $Q\bar{Q}$ photoproduced in a resolved photon interaction.

the photon remnants get out of the beam pipe and can be detected. Since it is not easy to reconstruct a jet from these particles because of their large angular spread, a method of studying the energy in the opposite direction to that of the hard jets was developed which allows to recognize the resolved photon events. One collects all the energy in a cone around the electron direction and by choosing the right aperture of this cone, and the right cut on the backward energy, $E_{\rm back}$, one obtains a clean sample of resolved photon events.

This study is based on Monte-Carlo events, generated with PYTHIA 5.5, for which the transverse momentum in the hard frame, $\hat{p}_T$, was bigger than 10 GeV/c. The jets were reconstructed using the LUCELL algorithm from JETSET 7.3. Only particles with an angle greater than 4° with respect to the beam pipe were considered, and only those events having 2 jets in the central region were accepted, the central region being defined by the pseudorapidity of the jet $|\eta_{jet}| \leq 2.7$. There is a clear difference between the two samples and by requiring $E_{\rm back} > 3$ GeVand at least one charged track in the backward direction, one obtains a sample which is almost completely populated by resolved photon events. Starting with a sample which has 77% of resolved photon events, one can enrich it with this algorithm to one having 99% resolved photon events (see table 3).

Table 3: Selection efficiency for resolved and direct photon events

reaction	σ(nb)	ϵ(%)	$\sigma_{\rm acc}$(nb)
Resolved γ	16.0	33	5.3
CQCD	1.4	1	0.014
PGF	3.4	1	0.034
fraction of resolved	0.77		0.99

3.3 Separation of direct photon subprocesses

The method [32,33] described in the previous section concentrates mainly on separating resolved photon events. Reference [34] makes an attempt to separate in addition also direct photon events. The jet search was done using the DECO algorithm [34], with the option of minimizing three functions: the covariant thrust in n directions, the sum of the jet masses, and the sum of the square of the jets masses.

An event is classified as a resolved photon event if 4–jets have been found by two of the three minimizing functions. In addition it has to fulfill some kinematical criteria, imposed on the definition of a resolved photon remnant jet [34]. An event is called a direct photon event if none of the 3 decomposition methods finds a resolved photon candidate.

A sample of events generated by PYTHIA 5.5 and having $\hat{p}_T$ >10 GeV/c were studied. Detector effects were included only by a beam pipe cut. Starting with a sample of 30% direct photon events, one can obtain a sample which contains close to 70% of them (Table 4). This method also enriches the resolved photon sample from

Table 4: Efficiency of resolved photon, photon–gluon fusion and CQCD event separation

reaction	σ(nb)(fraction(%))	fraction(%), direct sel	fraction(%), resolved sel
resolved photon	9.6 (70)	32	94
photon–gluon	2.9 (21)	48	4
CQCD	1.2 (9)	20	2

70% to 94%.

3.4 Separation of quark and gluon jets

In the previous section we have seen how one can achieve an enrichment of direct photon events from 30% to 70%. Let us assume that the method can be improved and that one can get an almost clean sample of direct photon events. This sample would contain photon–gluon fusion(PGF) events and Compton QCD events. We would like to have a method of separating these two classes of events. Isolating the photon–gluon events is necessary for gaining information on the gluon distribution of the proton [32], while from the CQCD sample one can learn about the sum of the quark densities in the proton.

In reference [35] an attempt is made to use a neural–network algorithm to separate gluon jets from quark jets. The program PYTHIA 5.5 was used to generate PGF and

CQCD events. Initial and final state parton showers were included and a cut of $p_T > 10$ GeV/c was imposed. Jets were reconstructed using the LUCELL algorithm and a beam pipe cut was performed. Only events with 2 well separated and coplanar jets in the central region were accepted.

The learning procedure was done with 22 variables. In addition to some individual jet variables like the transverse energy, the pseudorapidity, the azimuthal angle of the jet, and some combinations of these, some of the Fodor momenta [36] have been used. These latter ones have been chosen because it was found that they show differences in their distributions for quark and gluon jets. In addition to the 22 inputs, the network consists of one hidden layer and one output node denoted by y. A quark jet is identified by having y bigger than a threshold value (chosen as 0.5) and a gluon jet, by having y less than this threshold value. Figure 7 shows the distribution of the output node y for gluon and quark jets. Using this method one gets a success rate of ~70% in correctly

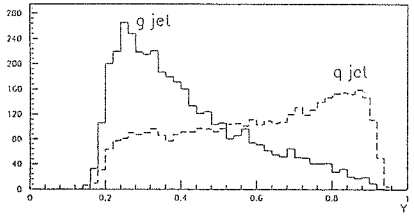

Figure 7: Distribution of the output node y for gluon jets (full line) and for quark jets (dashed line).

identifying the jet type (Table 6). These results are preliminary and more tuning has

Table 5: Jet classification results using a neural–network algorithm

	Generated partons					
Network	gluon	quark				
decision		$< q >$	QCDC		PGF	
			Light	Heavy	Light	Heavy
gluon	73%	32%	26%	40%	34%	42%
quark	27%	67%	74%	60%	66%	58%

to be done. Nevertheless, they are very encouraging.

4 Determination of gluon density

The usual way to get information about parton distributions is from fits to data of structure function measurements. Since however the structure functions depend only indirectly on the gluon density, our knowledge about the latter is very poor [37]. The gluons are especially important since they populate the region of low x, which gives the dominant contribution to interactions at high energies.

At HERA we have the unique opportunity to measure the gluon density directly by isolating events where the interaction is with the gluon at the partonic level, and then measuring the x of the gluon, x_g. The reader should however be cautioned that this interpretation is valid in leading order and gets more complicated once higher order corrections are considered. Setting this aside, one can get information about the gluon density in the proton by considering J/Ψ [38] or D^* [39] photoproduction in PGF events, and about the gluon density in the photon, by studying the DIC process [40].

4.1 Gluon density in the proton

4.1.1 J/Psi photoproduction

Though the J/Ψ can be photoproduced both through the direct photon reactions and through the resolved photon ones, the dominant contribution comes from the inelastic process $\gamma p \rightarrow J/\Psi X$ (figure 8). In the colour–singlet model [41] the differential cross

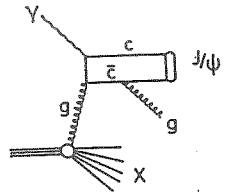

Figure 8: Diagram describing the inelastic photoproduction of J/Ψ.

section for this reaction is:

$$\frac{d\sigma}{dxdt} = G(x,\mu^2)\frac{d\hat{\sigma}}{dt} \tag{18}$$

where $G(x,\mu^2)$ is the gluon density function in the proton at the hard scattering scale μ, and $\hat{\sigma}$ is the cross section of the hard process $\gamma g \rightarrow J/\Psi g$. This model estimates a cross section of about 8.5 nb [38].

The variable x, which is actually x_g, can be determined by using the following relation [32]

$$x = \frac{\hat{s}}{ys}. \tag{19}$$

The y variable can be determined using the Jacquet–Blondel method, which uses all the observed hadrons in the detector, or from the scattered electron detected in the electron tagger of the luminosity monitor, and the square of the invariant mass of the γ–parton system, $\hat{s}$, has to be evaluated from the jet–jet invariant mass. Figure 9 shows that one can get a very good correlation between the generated gluon x and that reconstructed by the above formula, down to x values as low as 3×10^{-4}.

4.1.2 D^* photoproduction

Another method of gluon density determination is to use charmed hadron events produced via $ep \rightarrow ec\bar{c}X$. In order to tag these events one uses reconstructed D^* events [39].

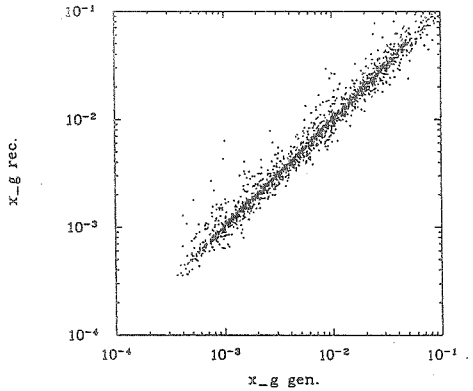

Figure 9: The generated x_g versus the reconstructed one for J/Ψ photoproduction via the diagram shown in figure 8.

The inclusive cross section has been estimated to be of the order of 1 nb, thus yielding a sample of about 10^5 charmed hadrons/100 pb^{-1}. Using the same method as above, one can then reconstruct the variable x_g. Figure 10 shows a similar correlation plot as that of figure 9, for inclusive $D^{*\pm}$ events as a tag of the charmed quark. As expected, the resolution that one obtains for these events is worse than that in the J/Ψ case. Note

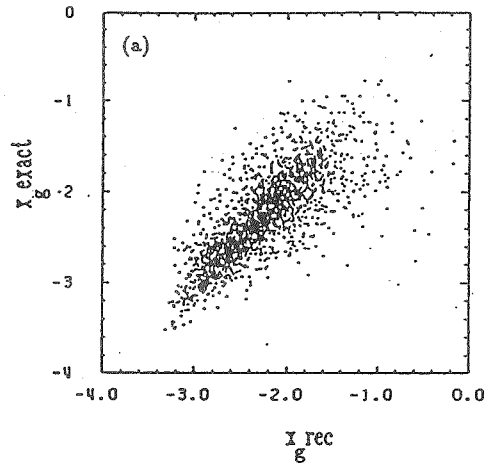

Figure 10: The generated x_g versus the reconstructed one using inclusive $D^{*\pm}$ photoproduction as a tag of the charmed quark.The numbers on the axis are powers of 10.

that in this method one needs to do a careful study of the background coming from the

resolved photon contribution, which is expected to contribute more in the D^* case than in that of the J/Ψ.

4.2 Gluon density in the photon

4.2.1 DIC process

The Deep Inelastic Compton (DIC) scattering process has been advocated [40] as a process through which one could get information about the gluon distribution both in the proton and in the photon. Prompt photons can be produced by the direct photon reaction $\gamma q \rightarrow \gamma q$, and by the resolved photon reactions $q^\gamma g^p \rightarrow \gamma q$ and $g^\gamma q^p \rightarrow \gamma q$ (see figure 11). The prompt high p_T photons produced by gluons from the photon

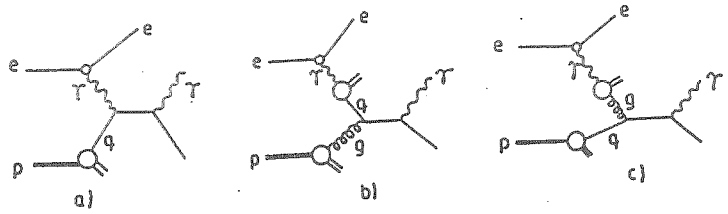

Figure 11: Direct (a) and resolved (b,c) photon diagrams contributing to the DIC process.

are expected to be very energetic, with energies up to 300 GeV. In addition they are expected to have a different rapidity distribution from those prompt photons produced by other partons.

It is shown in [42] that these high p_T prompt photons can be detected in spite of the background expected from photons produced as decays of other particles. By choosing photons with energies larger than 20 GeVand transverse momentum bigger than 5 GeV/c, the background can be reduced to as low as ~25%.

5 $\gamma\gamma$ reactions at HERA

The possibility of $\gamma\gamma$ reactions at HERA has been mentioned in earlier $\gamma\gamma$ workshops [43, 44], and recently in the HERA physics workshop [45,46]. One could isolate these reactions by studying muon pair production via $\gamma^e\gamma^p \rightarrow \mu^+\mu^-$. By using some some kinematic cuts to reduce the beam-gas background one expects to have about 1000 $\mu\mu$ events coming from $\gamma\gamma$ interactions for an integrated luminosity of 100 pb^{-1}.

Events with the scattered electron in the luminosity monitor and the two detected muons in the main detector will give a very clean sample for the extraction of the photon density of the proton. The momentum fraction x of the γ^p can be calculated from the experimental observables.

6 Summary and Conclusions

We are all eagerly awaiting the first results (expected and **unexpected**) of HERA.

Acknowledgements

I would like to thank H.Abramowicz for many illuminating discussions and for a critical reading of this summary. This work was partly supported by the German Israeli Foundation (GIF I-149-110.7/89).

References

[1] Proceeding of the HERA physics workshop, eds W.Büchmüller and G.Ingelman (1992).
[2] J.Bartels et al., in reference 1 (1992).
[3] J.Engelen et al., in reference 1 (1992).
[4] B.Schrempp et al., in reference 1 (1992).
[5] G.Altarelli, in reference 1 (1992).
[6] G.A.Schuler, in reference 1 (1992); A.Levy, in reference 1 (1992);
[7] T.H.Bauer et al., Rev Mod. Phys. 50, 261 (1978).
[8] H.Kolanoski, P.M.Zerwas, Two photon physics, in High Energy Electron Positron Physics, eds A.Ali and P.Söding (1988).
[9] J.J.Sakurai, Ann. Phys. 11, 1 (1960).
[10] H.Abramowicz et al., Parton distributions in the photon, DESY 91-057, accepted to J.Mod.Phys.A (1992).
[11] P.V.Landshoff, LP-HEP conference, Geneva, July, 1991.
[12] H.Abramowicz, E.Levin, A.Levy, U.Maor, Phys. Lett. 269B, 465 (1991).
[13] G.Schuler, J.Terron, in reference 1.
[14] M.Drees, F.Halzen, Phys. Rev. Lett. 62, 275 (1988).
[15] R.Gandhi, I.Sarcevic, Phys. Rev. D44, R10 (1991).
[16] J.R.Forshaw, J.K.Storrow, Phys. Lett. B268, 116 (1991).
[17] J.C.Collins, G.A.Ladinsky, Phys. Rev. D43, 2847 (1991).
[18] G.Wolf, Proc. 1971 Intern. Symp. on Electron and photon interactions at high energies (Cornell, 1971) p. 189.
[19] A. Levy, U. Maor, Phys. Lett. B182, 108 (1986).
[20] F.W.Brasse et al., Nucl. Phys. B110. 413 (1976).
[21] S.Levonian, in reference 1.
[22] M.Costa, K.Piotrzkowski, L.Suszycki, in reference 1.
[23] E.Lohrmann, in reference 1.
[24] C.F.Weizsäcker, Z. Phys. 88, 612 (1934); E.J.Williams, Phys. Rev. 45, 729 (1934).
[25] P.Kessler, Nouvo Cimento 17, 809 (1960).
[26] H.Uijterwaal, Second level trigger cuts for beam gas supression, ZEUS-note 01-049 (1991).
[27] J.R.Cudell, F.Halzen, C.S.Kim, Mod. Phys. A3, 1051 (1988).
[28] M.Drees, K.Grassie, Z. Phys. C28, 451 (1985).
[29] H.Abramowicz, K.Charchula, A.Levy, Phys. Lett. 269B, 458 (1991).
[30] A.Ali, D.Wyler, in reference 1 (1992).
[31] J.Smith, W.L.van Neerven, Stony Brook Report, ITP-
[32] G.D'Agostini, D.Monaldi, Z. Phys. C48, 467 (1990).
[33] A.Valkarova, in reference 1.

[34] G.Knies, in reference 1.
[35] G.Barbagli, G.D'Agostini, D.Monaldi, in reference 1.
[36] Z.Fodor, Phys. Rev. D41, 1726 (1990).
[37] H.Abramowicz et al., Mod. Phys. Lett. A6, 1361 (1991).
[38] H.Jung, G.A.Schuler, J.Terron, in reference 1 (1992).
[39] R. van Woudenberg et al., in reference 1 (1992).
[40] A.Bawa, M.Krawczyk, in reference 1.
[41] E.L.Berger, D.Jones, Phys. Rev D23, 1521 (1981).
[42] A.Levy, D.Revel, in reference 1.
[43] J.Field, $\gamma\gamma$ workshop, Aachen 1983.
[44] P.M.Zerwas, $\gamma\gamma$ workshop, Shoresh 1988.
[45] G.Levman, in reference 1.
[46] P.Bussey, in reference 1.